ACTA
AMAZONICA

# Mineralogical and geochemical influences on sediment color of Amazon wetlands analyzed by visible spectrophotometry

José Tasso Felix GUIMARÃES[1*], Marcelo Cancela Lisboa COHEN[2,3], Marlon Carlos FRANÇA[2], Any Kelly Terra da SILVA[2], Suyanne Flavia Santos RODRIGUES[2]

**ABSTRACT**

Based on sedimentological and geochemical data, this work relates spectrophotometric measurements with sediment composition and its application in palaeoecological studies of Amazon wetlands. The CIELAB values are directly related to mineralogical and chemical composition, mostly involving quartz, iron oxyhydroxides and sulfides (e.g. pyrite), and total organic carbon. Total organic carbon contents between 0.4-1%, 1-2%, 3-5% and 15-40% were related to L* (lightness) data of 27, 26-15, 7-10 and 7 or less, respectively. The CIELAB values of a deposit in Marabá, Pará, were proportional to variations in quartz and total organic carbon contents, but changes in zones of similar color, mainly in the +a* (red) and +b* (yellow) values of deposits in Calçoene, Amapá and Soure, Pará, indicate a close relationship between total organic carbon content and iron oxyhydroxides and sulfides. Furthermore, the Q7/4 diagram (ratio between the % reflectance value at 700 nm to that at 400 nm, coupled with L*) indicated iron-rich sediments in the bioturbated mud facies of the Amapá deposit, bioturbated mud and bioturbated sand facies of Soure deposit, and cross-laminated sand and massive sand facies of the Marabá core. Also, organic-rich sediments were found in the bioturbated mud facies of the Amapá deposit, lenticular heterolithic and bioturbated mud facies of the Soure deposit, and laminated mud and peat facies of the Marabá deposit. At the Marabá site, the data suggest an autochthonous influence with peat formation. The coastal wetland sites at Marajó and Amapá represent the development of a typical tidal flat setting with sulfide and iron oxyhydroxides formation during alternated flooding and drying.

**KEYWORDS:** Sedimentology, Amazon region, Munsell color systems, Mineralogy, chemical composition.

# Influências mineralógicas e geoquímicas na cor dos sedimentos das zonas úmidas da Amazônia analisada através da espectrofotometria no visível

**RESUMO**

Com base em dados sedimentológicos e geoquímicos, este trabalho relaciona medições espectrofotométricas com a composição do sedimento, e sua aplicação em estudos paleoecológicos das áreas alagáveis da Amazônia. Os dados CIELAB estão diretamente relacionados à composição mineralógica e química dos sedimentos, especialmente quartzo, oxihidróxidos e sulfetos de ferro, e carbono orgânico total. Conteúdos de carbono orgânico total entre 0,4-1%, 1-2%, 3-5% e 15-40% foram relacionados a dados de L* (luminosidade) de 27, 26-15, 7-10 e 7 ou menos, respectivamente. Os valores CIELAB de um depósito com turfa em Marabá, Pará, foram proporcionais a variações no conteúdo de quartzo e carbono orgânico total, mas mudanças nas zonas de cores similares, principalmente nos valores de +a* (vermelho) e +b* (amarelo), ao longo de outros depósitos em Calçoene, Amapá e Soure, Pará, indicam uma relação muito próxima entre os conteúdos de carbono orgânico total, oxihidróxidos e sulfetos de ferro. Além disso, o diagrama Q7/4 (razão entre valores percentuais de refletância em 700 nm e 400 nm, juntamente com dados de L*) indicou sedimentos ricos em ferro para a fácies lama bioturbada no depósito do Amapá, fácies lama bioturbada e areia bioturbada do depósito de Soure, e das fácies areia com laminação cruzada e areia maciça do depósito de Marabá. Ainda, sedimentos ricos em carbono orgânico foram encontrados na lama bioturbada no depósito do Amapá, fácies heterolítica lenticular e lama bioturbada do depósito de Soure, e das fácies lama laminado e turfa do depósito de Marabá. Na área de Marabá, os dados sugerem uma influência autóctone com formação de turfa. As áreas de zonas úmidas costeiras no Marajó e Amapá representam o desenvolvimento típico de planícies de maré com formação de sulfetos e oxihidróxidos de ferro durante alternâncias entre inundação e exposição.

**PALAVRAS-CHAVE:** Sedimentologia, Região Amazônica, Sistema de cor Munsell, Mineralogia, Composição química.

[1] Instituto Tecnológico Vale - ITV. Rua Boa Ventura da Silva 955, 3º andar, Umarizal, Belém (PA), Brasil. Phone: 55 91 32135561. E-mail: tasso.guimaraes@vale.com *Corresponding author

[2] Programa de Pós-Graduação em Geologia e Geoquímica, Universidade Federal do Pará. Rua Augusto Corrêa 1, Guamá, 66075-110 Belém, PA, Brasil

[3] Faculdade de Oceanografia, Universidade Federal do Pará. Rua Augusto Corrêa 1, Guamá, 66075-110 Belém, PA, Brasil

## INTRODUCTION

Geochemical analysis provides a variety of information about mineralogy, elemental or isotopic composition of carbonate, organic and siliciclastic sediments for paleoenvironmental reconstruction and climate studies. Most of these analyses are destructive, time-consuming, require specific equipment, complex and expensive. On the other hand, sediment color is considered an important qualitative parameter applied to describe and distinguish sedimentary facies, by its relation with mineralogical and chemical composition (Debret *et al*. 2011). Sediment color is frequently related to clastic (inherited) and diagenetic minerals, which are the products of climate, transport agents and physico-chemical conditions. Color mainly depends on the contents of organic carbon and iron, but also on the forms of iron: reddish and yellowish colors are usually associated to ferric ($Fe^{3+}$) hematite and goethite, whereas greenish-grayish colors indicate the presence of ferrous ($Fe^{2+}$) iron. High organic carbon contents related with anoxic conditions result in dark colors, and mottlings result from bioturbation and/or alternating ferric/ferrous forms on a centimeter scale (Tucker 2003).

A common method to measure sediment color relies on a visual comparison with color charts with the Munsell HVC (Hue, Value and Chroma) color system (Munsell Color 2009). In the Munsell system, color space is conceptualized as a cylinder where the perceptual attributes of color lightness (value or V) and saturation (chroma or C) are represented as linear coordinates, while the third dimension (hue or H) is represented as a polar coordinate. The hue scale is denoted by the letter abbreviation of the spectral color (R for red, YR for yellow-red, Y for yellow) preceded by numbers from 2.5 to 10. The value scale is specified on a numerical scale from 0 (absolute black) to 10 (absolute white). The chroma scale refers to the intensity of the color. It is described numerically beginning at 0 for neutral grey (the achromatic point) to a maximum of 20. In the rock-color chart (Munsell Color 2009), value and chroma range from 2 to 8 and 1 to 6, respectively. The measurement of sediment color using HVC system describes a perceptual color space and is not a quantitative measurement of visible light, and thus it is subject to errors due to the observer, ambient lighting, sample moisture and dirty color charts (Rossel *et al*. 2006). Nevertheless, it is sufficient for many purposes, but it is surprising how one sedimentologist's subjective impression of color can vary from another's (Tucker 2003). Thus, the use of instrumental methods to evaluate sediment color may be used to suggest insights about genetic processes acting on the depositional environment, since methods for chemical analysis of sediments are labor intensive and analytical costs become a limiting factor in most sedimentological research (e.g. Malley *et al*. 2000).

On the other hand, reflectance in the visible spectrum represented as color coordinates in the CIELAB (International Commission on Illumination $L^*a^*b^*$) system, dating from 1931, has given reliable results (e.g. Ortiz *et al*. 2009) for sediment study. Hering (1964) demonstrated that color stimuli in the retina can be translated into distinctions between light and dark ($L^*$ - lightness) ranging from 0 (absolute black) to 100 (absolute white), a red ($+a^*$) to green axis ($-a^*$), and a yellow ($+b^*$) to blue axis ($-b^*$). Uniform changes in the $L^*a^*b^*$ components correspond to uniform changes in perceived color, hence relative perceptual differences between any two colors can be approximated by treating each color as a point in the dimensional space and taking the Euclidean distance between them (Hering 1964). Many studies have thus used spectrophotometers to measure reflectance in small increments across a range of wavelengths, yielding a reflectance spectrum that can provide detailed information about the lithological and chemical composition of marine sediment cores of the Quaternary period (Balsam and Deaton 1996; Balsam *et al*. 1998; Leach *et al*. 2008).

The quantitative measurement of color may provide significant insights about substrate conditions during plant development and the formation of peat deposits. However, information about the application of this method to continental environments is still scarce (Malley *et al*. 2000). Plant growth, as well as extended flooding and waterlogging, influence diagenetic processes in tidal flats (Menezes *et al*. 2008). The presence of expansive clay minerals swell (e.g. smectites) reduces sediment permeability and further decreases oxygen supply, increasing carbon dioxide levels and decreasing sediment pH (Henderson and Patrick 1982; Berrêdo *et al*. 2008). Such conditions result in a set of unique and properties that can be evaluated by the analysis of color. Therefore, this work aimed a) to compare results using visual assessment versus spectrophotometry, b) to relate spectrophotometric measurements to sediment composition of Amazonian wetlands, and c) to assess the application of such techniques in palaeoecological studies of Amazon wetlands.

## MATERIALS AND METHODS

### Study Area

The studied wetlands are located in the eastern Amazon region near the cities of Calçoene (02º 36'10 N, 50º 50'05 W), in the State of Amapá, Soure (00º 40'26 S, 48º 29'02 W) and Marabá (05º 21'03 S; 49º 09'50 W) in the State of Pará (Figure 1A). The Amapá site presents extensive Holocene tidal flats, influenced by a semi-diurnal macrotidal regime (5-6 m amplitude) and the Amazon River's discharge (Meade et al. 1985; Gallo and Vinzon 2005), and is mainly colonized by herbaceous vegetation (Guimarães et al. 2010, Figure 1B). The

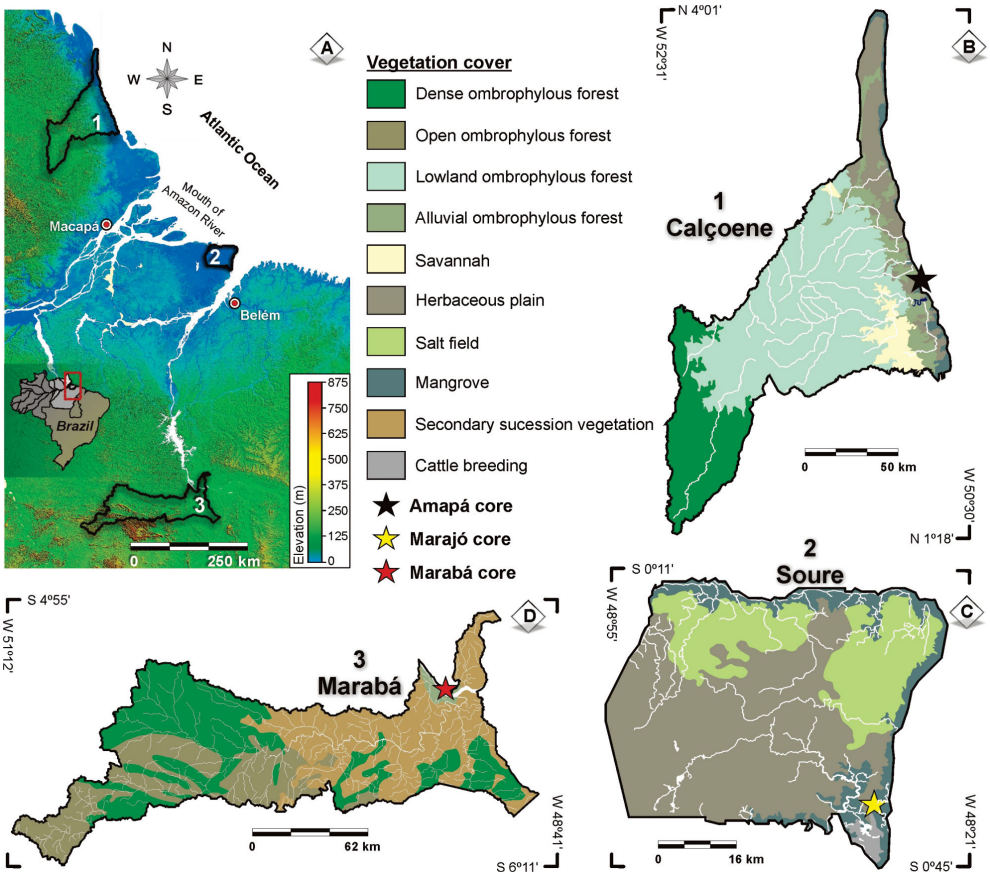


**Figure 1 -** Elevation map including the study sites (A), vegetation units and sampling sites in Amapá (B), Marajó (C) and Marabá (D). (Available in color in the electronic version).

herbaceous plain sampled is only flooded by a water column of 10 cm during overbank flow at higher spring tides of the rainy season (supratidal), and is characterized by an elevation between approximately 2 and 4 m and low drainage density due to the siltation of the tidal channels (Guimarães *et al.* 2012). The climate is Tropical/megathermal, characterized by a total annual precipitation of 3,000 mm, mostly concentrated in January to July and average temperature around 27.5 ºC (Bezerra et al. 1990). The Soure site comprises tidal flats with mangrove vegetation (Figure 1C), submitted to a semi-diurnal macrotidal regime of ~4 m range. These mangroves are restricted to the coastline, colonizing intertidal flats of wider tidal channels. This region presents total annual precipitation of 2,550 mm and average temperature about 26.5 ºC (Moraes et al. 2005). The Marabá site is a Holocene alluvial plain colonized by alluvial ombrophylous forest located between the Itacaiúnas and Tocantins Rivers (Figure 1D). The annual precipitation is 2,116 mm and average temperature is 26.3 ºC (Fisch et al. 1998).

## Sampling and Facies Description

Sediment cores were collected to a depth of 1 m using a Russian Sampler, and consisted of grayish mud and yellowish sand with 1 kg each. Following the proposal of Walker (1992), facies analyses included descriptions of lithology and structures. X-ray radiographs aided in the identification of sedimentary structures. The sedimentary facies were codified following Miall (1978).

Visual assessments of color were made in the laboratory under diffuse natural daylight using Munsell color charts (Munsell Color 2009). An spectrophotometer (Spectrolino : SpectroScan, Neu-Isenburg, Germany) under a D65 illuminant (calibrated with a white ceramic plate) was used to obtain *L*a*b** data for each 1 cm interval along the surface of the sediment cores in the laboratory at dark conditions. The cores were statistically subdivided into zones of similar color based on Ward's linkage of CIELAB data by the Euclidean distances method. Additionally, *L*a*b** data were obtained from each chip of the Munsell chart used in the description above using a portable spectrophotometer

(Spectrolino: SpectroScan, Neu-Isenburg, Germany, with D65 illuminant, operating at visible spectrum). Calibration of the spectrophotometer was performed using a white ceramic plate (reflectance of 100%). Additionally, the data were compared with automatic conversions between the color space models provided by BabelColor 3.0 (BabelColor 2010). The repeatability of color measurements, determined by the standard deviation of successive measurements, was less than 0.05 CIELAB units. Furthermore, the Q7/4 ratio (the ratio between the % reflectance value at 700 nm to that at 400 nm) which provides the numerical description of the general slope of visible spectrum. Coupled with $L^*$, it constitutes the Q7/4 diagram, which was applied to identify the characteristic signatures of the main sediment constituents in the wetland deposits (Debret et al. 2011).

### Mineralogical and chemical analysis

The identification of minerals was achieved using a diffractometer (PW 3040, PANalytical, Almelo, The Netherlands), with a copper anode (kα1 = 1,54060 Å), tension generator and current adjusted to 40 kV and 30 mA, respectively. Diffractions of total samples were obtained in the range of 5 to 75º 2θ, with step size 0,02º - 10s. The results were interpreted using the X'Pert HighScore 2.1 software and the International Center for Diffraction Data database, and are presented as mineral symbols following Kretz (1983).

The chemical composition was analyzed from a 0.2 g sample by inductively coupled plasma optical emission spectrometry (ICP-OES) using a Spectro Ciros Vision ICP - (Spectro Analytical Instrument, Mahwah, NJ) spectrometer following lithium metaborate/tetraboratate fusion and dilute nitric digestion on an Acme Analytical Laboratory, Vancouver, Canada. Total sulphur (TS) and total organic carbon (TOC) were obtained from a LECO CS-300 combustion analyzer. The average contents of major components and trace elements were normalized to the Upper Continental Crust (Wedepohl 1995), Post-Archean Australian Shales (Turekian and Wedepohl 1961) and other tidal mud flats colonized by mangrove vegetation (Djuwansah 1990; Costa *et al.* 2004; Vilhena *et al.* 2010). Similarity analyses between chemical data were performed by Single Linkage and Pearson product-moment correlation coefficient (ρ, Stigler 1989), where ρ values of 1 and -1 denote perfect positive and negative correlation between x and y, respectively.

## RESULTS

### Comparison between Munsell notation and Cielab color measurements

The $L^*a^*b^*$ results of Munsell chips revealed as expected a strong relationship between Munsell V and $L^*$, as both represent the same color property (lightness). Munsell V of 8, 7 and 6 gave $L^*$ numbers ranging from 86.2 to 78.8 ($\bar{x}$ = 81.7), 79.4 to 52.8 ($\bar{x}$ = 74.3) and 74.7 to 63.3 ($\bar{x}$ = 69.6), respectively. Munsell V of 5, 4 and 3 gave $L^*$ numbers between 66.3 and 57.9 ($\bar{x}$ = 61.8), 63.4 and 50.3 ($\bar{x}$ = 54.1) and 53.5 and 46.9 ($\bar{x}$ = 50.4), respectively. The lowest $L^*$ data, between 54.8 and 37 ($\bar{x}$ = 46.5), were obtained for the V of 2. Redder hues (5R and 10R) resulted in positive $a^*$ data near 8.3, whereas yellower hues (5Y and 10Y) gave negative $a^*$ data ~ -1.1. Yellower hues had higher $b^*$ data than redder hues (approximately 16.6 and 3.8 respectively). The $-a^*$ data are associated with relatively high deviation from the green axis of the CIELAB system. In general, the lowest $a^*$ and $b^*$ data are associated to bluish and greenish Munsell colors. The positive $a^*$ and $b^*$ data suggest the predominance of red and yellow axes in the CIELAB system.

### Sedimentary facies, color description, mineralogy and geochemistry

#### Herbaceous plain deposit, Amapá site

The herbaceous plain deposit presents mud with fresh roots of herbaceous plants (facies Mbh; Table 1), and slight to intense bioturbation with dwelling structures of benthic fauna. Three zones of similar color were identified by spectrophotometric analysis with major oscillations of $+b^*$ (yellow) values (Figure 2). This classification largely differs from the five segments described visually (Table 2), and the discrepancy is mainly due to biased perception of mottlings and the underestimation of the influence of the $-a^*$ (green) and $+a$ (red) axes in the visual and CIELAB systems, respectively.

The minerals included quartz, kaolinite, anatase, muscovite, albite and K-feldspar (Figure 2A). The major components were $SiO_2$ (59-65%), $Al_2O_3$ (15-17%), $Fe_2O_3$ (5-8,6%), $K_2O$ (2.3-2.6%), MgO and $Na_2O$ (1.2-1.5%), $TiO_2$ (~0.8%), CaO (0.4-0.6%), $P_2O_5$ (~0.1%) and MnO (0.3%). In general, the trace elements occurred in a homogeneous pattern along the core, except for Ba and Sr that slightly decreased from the bottom to the top. Also, Ba content was higher than in other tidal mud flats in the Amazon (Table 3). Total organic carbon and sulfur were found at low concentrations (~0.3% and 0.05%, respectively) in the 100 to 30 cm interval, slightly increasing to 1.3% and 0.7%, respectively in the shallower layer (Figure 2B).

The correlation coefficient between $SiO_2/Al_2O_3$ (-0.72) indicates a quartz/clay antagonism. Additionally, the coefficient between $SiO_2$/Zr (0.78) indicates the presence of zircon in the sand fraction of the sediment. $SiO_2$ and $Al_2O_3$ are the most abundant components, comprising quartz, diatom shells (Costa *et al.* 2004) and clay minerals (kaolinite). The slight upward depletion of $Na_2O$, MgO, CaO, Ba and Sr likely indicates a decrease in sea water influence (Figure 2B). The

**Table 1 -** Summary of facies descriptions and sedimentary process in the sediment cores.

| Facies | Description | Process |
|---|---|---|
| Massive sand (Sm) | Moderately sorted, medium sand with some root marks. | The massive nature may indicate a rapid sedimentation or produced during drilling. Thus, the deposit could be in part stratified. |
| Cross-laminated sand (Sc) | Moderately sorted medium to fine sand with some roots and root marks. | Migration of small ripples during relatively low energy, unidirectional flows. |
| Laminated mud (Mb) | Mud with parallel lamination, roots, root marks and plant debris. | Very low energy flows with mud deposition from suspension during overbank flow. |
| Peat (Pt) | Peat material with decomposed and intact vegetable fibers. Some crystals present pale brass-yellow hue. | Stagnant and reduced conditions with vegetable tissues as the main source of the deposit. The colored crystals can be associated to the presence of pyrite. |
| Lenticular heterolithic (Hl) | Mud with single flat lenses of rippled fine- to very fine sand. Convolute lamination can be locally found. | Low energy flows with mud deposition from suspension, but with periodic sand inflows through migration of isolated ripples. Convolute lamination was produced by localized differential forces acting on a hydroplastic sediment layer |
| Bioturbated mud (Mbh and Mb) | Mud with many roots, root marks, roots traces in growth position and benthic tubes. Locally, herbaceous roots can be identified. | Diffused mixture of sediments and alternating colors by intense bioturbation and diagenetic process, respectively. |
| Bioturbated sand (Sb) | Fine to very fine sand with many roots and root marks. | Sand transported by overflow fluxes during spring tides and mixed by root development. |

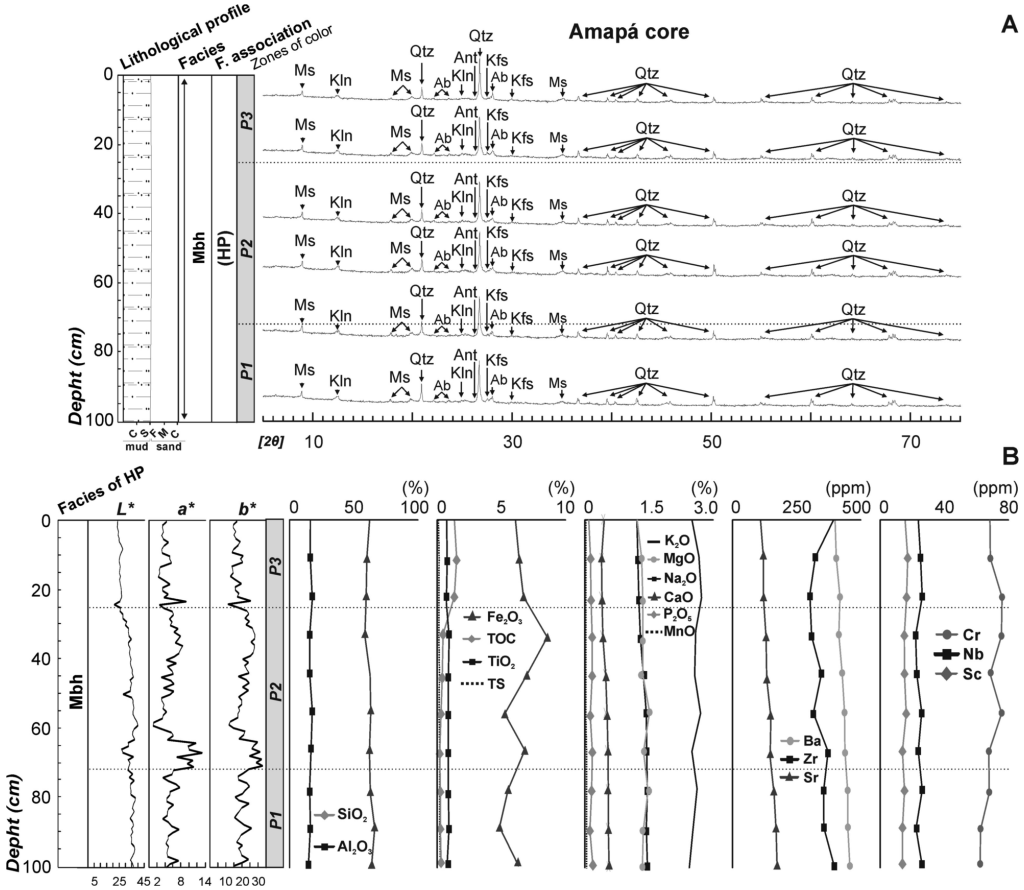


**Figure 2 -** X-ray diffraction patterns showing the main minerals (A) and concentration profiles of major components and trace elements of the Amapá core (B). CSFMC at the basis of the core means Clay, Silt to mud size and Fine, Medium and Coarse to sand size.

**Table 2 -** Comparison between Munsell HVC (visual descriptions of color) and CIELAB color measurements (spectrophotometric identification of color) of sediment cores from Amazon wetlands.

| | Visual descriptions | | Spectrophotometric analysis | | | | | | | |
|---|---|---|---|---|---|---|---|---|---|---|
| | Segments (cm) | HVC data | HVC TO CIELAB | | | Segments (cm) | CIELAB data (x̄) | | | Zones of color |
| | | | L* | a* | b* | | L* | a* | b* | |
| AP | 30-0 | 10G 4/2 (grayish green) | 52.7 | -36 | 3.2 | 0-25 | 25.1 | 3.9 | 16.4 | P3 |
| | 45-30 | 10YR 6/2 (pale yellowih brown) | 70.8 | 1.0 | 10.5 | 25-73 | 33.2 | 6.8 | 23.8 | P2 |
| | 63-45 | 10GY 7/2 (pale yellowish green) | 74.3 | -4.1 | 2.4 | | | | | |
| | 75-63 | 10YR 6/2 (pale yellowih brown) | 70.8 | 1.0 | 10.5 | 73-100 | 35.2 | 4.9 | 19.0 | P1 |
| | 75-100 | 10GY 7/2 (pale yellowish green) | 74.3 | -4.1 | 2.4 | | | | | |
| MJ | 50-0 | 10R 4/2 (grayish red) | 52.2 | 5.4 | 6.6 | 0-40 | 29.1 | 7.7 | 21.0 | J3 |
| | 70-50 | 10Y 7/4 (moderate greenish yellow) | 75.9 | -2.9 | 21.4 | | | | | |
| | 70-100 | 10GY 5/2 (grayish green) | 60.4 | -7.2 | 15.9 | 40-80 | 24.7 | 5.2 | 17.9 | J2 |
| | | | | | 80-100 | 22.0 | 2.4 | 8.9 | J1 | |
| MB | 35-0 | 10R 2/2 (very dusky red) | 38.4 | 6.0 | 3.7 | 0-45 | 7.4 | 3.8 | 5.8 | B3 |
| | 35-45 | N1 (black) | 40.5 | -0.3 | 1.7 | | | | | |
| | 45-55 | 10Y 5/4 (light olive) | 63.9 | -4.2 | 29.2 | 45-55 | 16.4 | 3.1 | 5.8 | B2 |
| | 55-100 | 5Y 6/4 (dusky yellow) | 71.1 | -0.4 | 12.2 | 55-100 | 31.4 | 5.1 | 14.8 | B1 |

high contents of $Fe_2O_3$ and weak coefficient between $Fe_2O_3$/*Cr (0.44) and* $Fe_2O_3$/total sulfur (-0.04) are consistent with *iron oxyhydroxides,* most likely goethite as suggested by the yellowish hues (Table 2), formed during prolonged subaerial exposure (Berrêdo *et al*. 2008).

The major and trace element composition is very similar to that in French Guiana and Bragança, Pará, mangroves, which are relatively enriched in $Fe_2O_3$ and immobile elements Sc, Zr, Nb and Cr in relation to Upper Continental Crust and Post-Archean Australian Shales (Table 3). The presence of albite and muscovite also indicates some contribution of Precambrian crystalline rocks from the Guianas Shield found near the coastal plain of the State of Amapá (Guimarães *et al*. 2012).

Other studies focused on the tidal flats of the northern Brazilian coast have also shown the predominance of quartz and kaolinite, but also smectite, illite, pyrite, jarosite, halite, muscovite, feldspar, albite, vermiculite and vermiculite-chlorite (Costa et al., 2004; Berrêdo *et al*. 2008; Vilhena *et al*. 2010).

**Mangrove deposit, Soure site**

The mangrove core consisted of mud with lenses of rippled sand (facies Hl; Table 1) that indicate low energy flow with mud deposition from suspension and periodic sand inflows, mostly through the migration of isolated ripples. This core also displayed convolute lamination, and many bioturbation features (facies Mb and Sb; Table 1) such as roots, root marks and dwelling structures produced by benthic fauna. Three zones of similar color were identified by visual and spectophotometric analysis, but the *-a** (green) and very high *+b** (yellow) values found with HVC color chips indicated an overestimation of the green and yellow axes in the CIELAB system (Table 2). Facies Mb had at least two main color zones that differ in *+a** (red) and *+b** (yellow) axis influence.

The minerals identified included quartz, kaolinite, anatase, muscovite, albite, K-feldspar and pyrite. However, pyrite was only found in facies Hl (Figure 3A). The samples mainly contained $SiO_2$ (73-81%), $Al_2O_3$ (7.3-9.9%), $Fe_2O_3$ (1.8-3.4%), $K_2O$ (1.5-1.8%), $Na_2O$ (0.8-1.0%), $TiO_2$ (~0.8%), MgO (0.5-0.7%) and CaO (~0.4%), $P_2O_5$ (0.05-0.08%) and MnO (0.02%). The trace elements occurred in a homogeneous pattern along the core, with the exception of Ba and Sr which decreased slightly from facies Hl to Sb. Total organic carbon and sulfur contents decreased from 2.2% and ~0.7% in facies Hl to 0.1% and 0.05% in facies Sb, respectively (Figure 3B). $SiO_2$ and $Al_2O_3$ were the most abundant components, in the form of quartz, clays, feldspars and micas. Two zones with distinct chemical and mineralogical characteristics can be identified based on the high contents of $Fe_2O_3$ (Figure 3A, B):

**Table 3 -** Comparison between the chemical composition of sediment samples of this study, Upper Continental Crust – UCC, Post-Archean Australian Shales – PAAS and other tidal mud flats colonized by mangrove vegetation.

| **Major (%)** | $SiO_2$ | $Al_2O_3$ | $Fe_2O_3$ | $K_2O$ | $Na_2O$ | MgO | CaO | $TiO_2$ | $P_2O_5$ | MnO | TOC | TS |
|---|---|---|---|---|---|---|---|---|---|---|---|---|
| Amapá [a] | 62.0 | 16.1 | 6.4 | 2.5 | 1.4 | 1.4 | 0.5 | 0.8 | 0.21 | 0.03 | 0.6 | 0.05 |
| Marajó [a] | 77.4 | 8.8 | 2.7 | 1.7 | 0.9 | 0.6 | 0.4 | 0.8 | 0.06 | 0.02 | 1.6 | 0.3 |
| Marabá [a] | 80.0 | 6.2 | 0.3 | 0.03 | 0.01 | 0.04 | 0.04 | 0.9 | 0.11 | 0.01 | 5.0 | 0.04 |
| Marapanim [b] | 52.7 | 19.1 | 6.9 | 1.5 | 1.4 | 1.0 | 0.4 | 0.7 | - | - | - | - |
| Bragança [c] | 55.1 | 15.1 | 5.2 | 1.4 | 2.6 | 1.4 | 0.4 | 0.6 | - | 0.02 | - | - |
| Guiana [d] | 55.2 | 18.5 | 6.0 | 2.6 | 1.6 | 1.7 | 0.4 | 0.8 | - | - | - | - |
| UCC [e] | 64.9 | 14.6 | 4.4 | 3.5 | 3.5 | 2.2 | 4.1 | 0.5 | 0.1 | 0.07 | - | - |
| PAAS [f] | 62.8 | 18.9 | 6.5 | 3.7 | 1.2 | 2.2 | 1.3 | 1.0 | 0.2 | 0.1 | - | - |
| **Trace (ppm)** | Zr | Ba | Sr | Nb | Cr | Sc | | | | | | |
| Amapá [a] | 348 | 416 | 138 | 24 | 69 | 15 | | | | | | |
| Marajó [a] | 592 | 361 | 98 | 17 | 41 | 8.3 | | | | | | |
| Marabá [a] | 558 | 52 | 18 | 19 | 27 | 3.9 | | | | | | |
| Marapanim [b] | 252 | 240 | 91 | 15 | 87 | 16 | | | | | | |
| Bragança [c] | 361 | 248 | 140 | 18 | 78 | - | | | | | | |
| Guiana [d] | 380 | 380 | 119 | - | 82 | 17 | | | | | | |
| UCC [e] | 237 | 668 | 316 | 26 | 12 | 7.0 | | | | | | |
| PAAS [f] | 210 | 650 | 200 | 19 | 23 | 16 | | | | | | |

[a] Sediment samples from Amazon wetlands (this study).
[b] Marapanim mangroves (Vilhena *et al*. 2010).
[c] Mangrove of the north eastern state of Pará (humid climate) after Costa *et al*. (2004).
[d] Mangrove of tropical and equatorial climate after Djuwansah (1990).
[e] Upper Continental Crust – UCC after Wedepohl (1995).
[f] Post-Archean Australian Shales – PAAS modified after Turekian and Wedepohl (1961).

in facies Hl, the samples contain higher levels of total organic carbon and total sulfur, and coefficients between $Fe_2O_3$/total sulfur (0.99) and $Fe_2O_3$/Cr (0.57) suggest a sulphate reduction zone that allowed pyrite formation. Moving upward towards facies Sb, the lower total organic carbon and sulfur contents, as well as coefficients between $Fe_2O_3$/total sulfur (-0.55) and $Fe_2O_3$/Cr (0,62) correspond to iron oxyhydroxides derived from the oxidation of pyrite, resulting in the grayish red colors (Table 2) (Vilhena *et al.* 2010).

The contents of major and trace elements are comparable to those from Marapanim mangroves, and generally enriched in $SiO_2$, Zr and Cr in relation to Upper Continental Crust and Post-Archean Australian Shales (Table 3). The presence of quartz, kaolinite and anatase, and the contents of $Fe_2O_3$ and $TiO_2$ suggest weathered products of Barreiras and Post-Barreiras sediments as a partial source to the deposit (e.g. Rossetti 2001; Rossetti *et al.* 2010). However, the presence of albite and muscovite indicates the contribution of Precambrian crystalline rocks from the Central Brazil Shield (e.g. Costa *et al.* 2004).

**Alluvial deposit, Marabá site**

This deposit presented massive and cross-laminated sands (facies Sm and Sc). The upper segments consisted of laminated mud (facies Ml) and peat material (facies Pt), as shown in Table 1. In the color analysis, four segments were recognized visually, but only three zones of similar color were identified through spectrophotometric measurements. Additionally, the CIELAB data of the sediment samples varied widely in relation to the CIELAB data of Munsell chips, mainly in the $L^*$ (lightness) color axis (Table 2). The color zones closely followed changes in sedimentary facies (Figure 4).

The X-ray diffraction analysis identified quartz, kaolinite, anatase and pyrite in the Marabá core. However, pyrite was restricted to facies Ml and Pt (Figure 4A). The samples were mainly composed of $SiO_2$ (55-95%), $Al_2O_3$ (1.7-13%), $TiO_2$ (0.6-1.5%) and $Fe_2O_3$ (0.2-0.5%). They also contained lesser amounts of $P_2O_5$ (0.05-0.25%), CaO (0.01-0.1%), MgO (0.02-0.07%), $K_2O$ (0.01-0.04%), $Na_2O$ (<0.02%) and MnO (<0.01%). The contents of trace elements except Zr increased, toward facies Pt. Total organic carbon and sulfur occur at low concentrations (~0.1% and 0.03%, respectively) in facies Sm, increasing to 39% and 0,1% in facies Pt, respectively (Figure 4B).

The contents of $SiO_2$ decrease from facies Sm to facies Pt and are inversely proportional to $Al_2O_3$ and total organic carbon, reflecting the importance of kaolinite in the Pt facies,

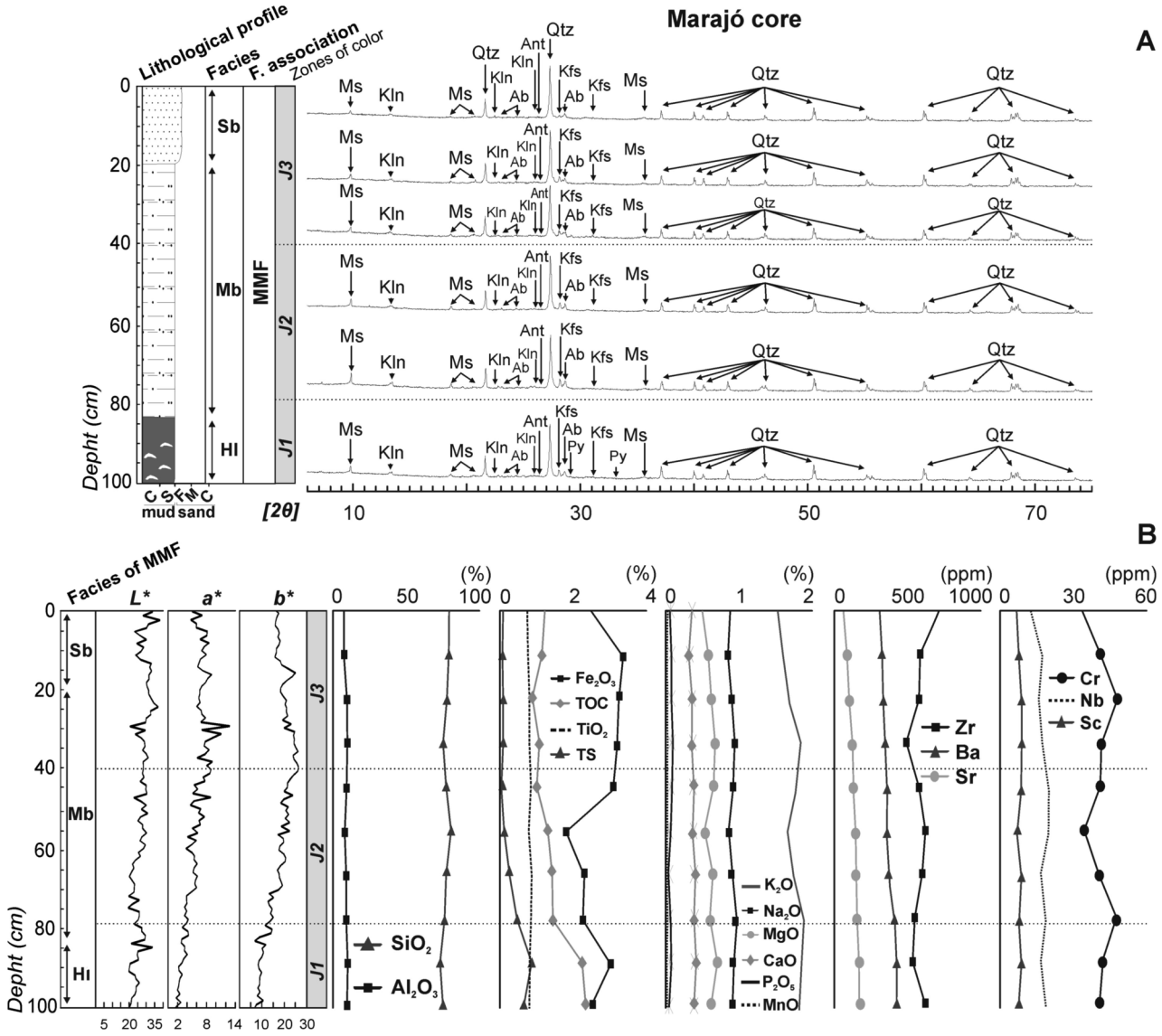


**Figure 3 -** X-ray diffraction patterns showing the main minerals (A) and concentration profiles of major components and trace elements of the Marajó core (B). CSFMC at the basis of the core means Clay, Silt to mud size and Fine, Medium and Coarse to sand size.

and of quartz below and organic matter than the quartz/sand fraction. The correlation coefficient between $SiO_2$/$Al_2O_3$ (-0.95) reinforce the quartz/clay antagonism. The $TiO_2$ contents and the coefficient between $TiO_2$/Nb (0.97) are well correlated with anatase, most likely derived from quartzarenites with tourmaline, zircon, staurolite, rutile, anatase and kyanite of the Itapecuru Group (e.g. Nascimento and Góes 2007), found near the Marabá site. The Zr/Sc coefficient (0.98) may be related to a source of igneous rocks that extends throughout the city of Marabá (Rossetti and Truckenbrodt 1997; CPRM 2010).

High contents of $Fe_2O_3$, $P_2O_5$ and total sulfur in facies Ml and Pt and the coefficient between $Fe_2O_3$/total sulfur (0.78) and $Fe_2O_3$/Cr (0.93) may indicate a reduction zone that promoted the in situ formation of pyrite (Figure 4A, B). Furthermore, $P_2O_5$, CaO and MgO also increase toward the top of the core and their coefficients with total organic carbon (0.88, 0.93, 0.75, respectively) as well as the $K_2O$/total organic carbon (0.63) suggests some binding to organic matter, especially of P as organic phosphate forms. The relative enrichment in $SiO_2$ and very low contents of CaO, $K_2O$, $Na_2O$ and MgO in relation to Upper Continental Crust and Post-Archean Australian Shales reflect the intense weathering degree of this sediment (Table 3).

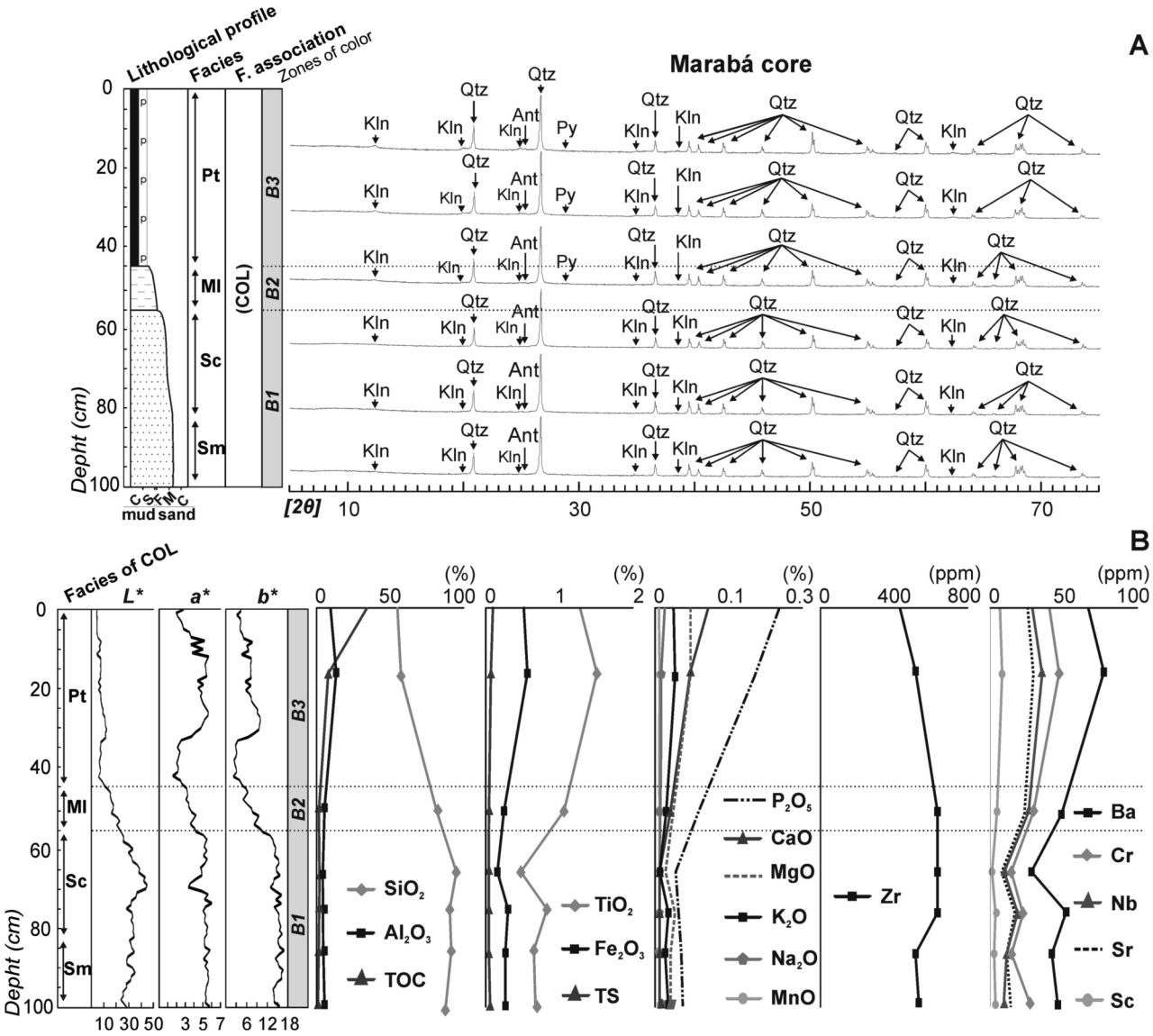


**Figure 4 -** X-ray diffraction patterns showing the main minerals (A) and concentration profiles of major components and trace elements of the Marabá core (B). CSFMC at the basis of the core means Clay, Silt to mud size and Fine, Medium and Coarse to sand size.

## DISCUSSION

### Cielab color system and its relationship with wetland sediments

The color of Amazon wetland sediments studied here can be attributed to the mineralogical and chemical composition of the sediment samples, including quartz, iron oxides and oxyhydroxides, free ferrous iron, as well as organic carbon content (Figure 2, 3, 4 and 5). Total organic carbon contents between 0.4-1%, 1-2%, 3-5% and 15-40% are related to $L^*$ (lightness) data of 27, 26-15, 7-10 and 7 or less, respectively, resulting in strong negative correlation (r~0.9). Lower $L^*$ occurs in zones B2 (facies Ml) and B3 (facies Pt) in the Marabá deposit, and zones J1 (facies Hl and part of facies Mb) in the Soure deposit (Figures 3 and 4, Table 2). These low $L^*$ values are primarily attributed to high organic carbon contents, which typically darkens sediments and soils. When total organic carbon contents exceed 2%, it may mask absorption features of other constituents of the deposit (e.g. Galvão and Vitorello 1998; Demattê and Garcia 1999; Fernandes *et al.* 2004). Furthermore, the lower $+a^*$ (red) and $+b^*$ (yellow) data in these color zones are well correlated to iron sulfide zone.

The CIELAB data of the Marabá core are proportional to variations in quartz and total organic carbon contents (Figure 4). Also, variations in $+a^*$ (red) and $+b^*$ (yellow) data along the different color zones of this and the Amapá core indicate

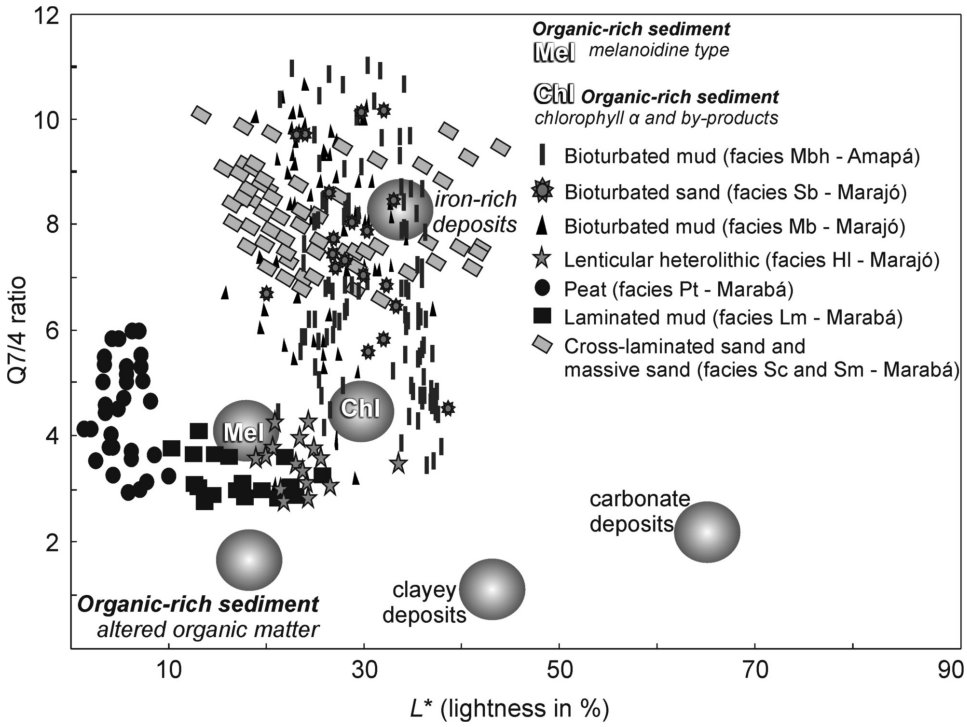


**Figure 5 -** Diagram of the relationship between the % reflectance value at 700 nm to that at 400 nm coupled with *L** (Q7/4 ratio), and *L** (lightness in %), which constitutes the Q7/4 of facies and main components of wetland sediments of the study site.

a close relationship between iron oxyhydroxides and total organic carbon content. However, only +*a** (red) and +b* (yellow) data ≥ 4 and 10, respectively, and *L** (lightness) data ≥ 24 are related to a major influence of iron oxyhydroxides. Lalonde *et al*. (2012) propose that the associations between organic carbon and iron formed mainly by co-precipitation and/or direct chelation promote the preservation of organic carbon in sediments, since sedimentary organic matter is not spread evenly over clay particles but covers a small surface area, and so iron or iron oxides provide cohesion to these compounds, fixing them to clay particles by covalent bonds.

Regarding the Q7/4 diagram (Figure 5), the Mbh facies of the Amapá core presented ratios between 4 and 11, and *L** (lightness) data from 20 to 40, which corresponds to iron- and organic-rich sediments. Facies Hl and Mb facies of the Soure core showed 700/400 ratios from 2 to 5, and *L** data from to 18 to 30 mainly related to organic-rich sediments, but Mb facies with 700/400 ratios from 6 to 11 also corresponded to iron-rich sediments as well as for the Sb facies. The Sc and Sm facies of the Marabá core showed 700/400 ratios between 6 to 10, and *L** data from 10 to 45, indicative of iron-rich deposits, while Ml and Pt facies mainly presents organic-rich sediments.

Variations in sediment color correlated with CIELAB data only occur along the facies Mb and Mbh (Figures 2, 3 and 5), mainly due to bioturbation processes (e.g. root activity). Indeed, oxidation of the rhizosphere by leakage of oxygen from roots of adapted species occurs when more oxygen is supplied than required for root respiration, thereby forming oxidized rhizospheres. Additionally, prolonged exposure of tidal flats may also allow the development of such alternations of color zones (Tinner 1999). Otherwise, color zones of the Marabá core consistently follow changes in lithology, from quartz sands (facies Sm and Sc) to peat (facies Pt), which may indicate partially syngenetic development since pyrite was formed during continuous organic input under stagnant water conditions. Therefore, extended flooding and waterlogging may form deposits with high content of organic matter and iron sulfide, while bioturbation processes allow the formation of iron oxyhydroxides zones and mottlings.

## CONCLUSIONS

The comparison between visual analysis based on Munsell and instrumental analysis based on CIELAB system revealed a generally biased color perception of mottlings by human eye. However, without mottling effect, the color zones of sediment cores closely follow changes in sedimentary facies. Based on spectrophotometric measurements, the sediment colors of Amazon wetlands are directly related to its mineralogical and chemical composition including quartz, iron oxyhydroxides, and organic carbon content. Regarding the organic carbon, total organic carbon contents between 0.4-1%, 1-2%, 3-5% and 15-40% were related to *L** (lightness) data of 27, 26-

15, 7-10 and 7 or less, respectively. Lower $L^*$ (lightness) of facies Ml (laminated mud) and facies Pt (peat) of the Marabá deposit, and facies Hl (lenticular heterolithic) and part of facies Mb (bioturbated mud) of the Soure deposit, which are attributed to high organic carbon contents. Otherwise, variations in $+a^*$ (red) and $+b^*$ (yellow) data along the different color zones of the Marabá and Amapá cores suggest a relationship between iron oxyhydroxides and total organic carbon content. Nevertheless, only $+a^*$ (red) and +b* (yellow) data ≥ 4 and 10, respectively, and $L^*$ (lightness) data ≥ 24 are mainly related to iron oxyhydroxides zones and mottlings. Therefore, spectrophotometric measurements can provide significant information about substrate conditions during plant development and the formation of peat deposits.

## ACKNOWLEDGEMENTS

This work was funded by CNPq (Project 562398/2008-2). The second author holds a scholarship from CNPq (Processes 302943/2008-0). The authors thank the members of the Laboratório de Dinâmica Costeira - Universidade Federal do Pará, Instituto Tecnológico Vale, and especially to associated editor and reviewers from Acta Amazonica to numerous comments and suggestions that helped to significantly improve this manuscript.

## REFERENCES

BabelColor. 2010. BabelColor CT&A 3.0.0 for Windows. The BabelColor Company. (http://www.babelcolor.com/main_level/download.htm). Accessed on 09/06/2010.

Balsam, W.L.; Deaton, B.C. 1996. Determining the composition of late Quaternary marine sediments from NUV, VIS, and NIR diffuse reflectance spectra. *Marine Geology*, 134: 31-55.

Balsam, W.L.; Deaton, B.C.; Damuth, J.E. 1998. The effects of water content on diffuse reflectance spectrophotometry studies of deep-sea sediment cores. *Marine Geology*, 149: 177-189.

Berrêdo, J.F.; Costa, M.L.; Vilhena, M.P.S.P.; Santos, J.T. 2008. Mineralogia e geoquímica de sedimentos de manguezais da costa amazônica: o exemplo do estuário do rio Marapanim (Pará). *Revista Brasileira de Geociências*, 38: 26-37.

Bezerra, P.E.L.; Oliveira, W.; Regis, W.D.E.; Brazão, J.E.M.; Gavinho, J.; Coutinho, R.C.P. 1990. Amazônia legal: zoneamento das potencialidades e dos recursos naturais. In: Instituto Brasileiro de Geografia e Estatística, Superintendência de Desenvolvimento da Amazônia. Projeto zoneamento das potencialidades dos recursos naturais da Amazônia: geologia, solos e vegetação. Rio de Janeiro: IBGE, div. 5, p. 9-89.

Costa, M.L.; Behling, H.; Berrêdo, J.F., Carmo, M.S.; Siqueira, N.V.M. 2004. Mineralogical, geochemical and palynological Studies of late Holocene Mangrove Sediments from Northeastern Pará State. Brazil. *Revista Brasileira de Geociências*, 34: 479-488.

CPRM. 2010. Geological information system. Brazilian Geological Service. On line dataset, Folhas NA/SA-22 23 MB, (http://geobank.sa.cprm.gov.br/.). Accessed on 27/08/2010.

Debret, M.; Sebag, D.; Desmet, M.; Balsam, W.; Copard, Y.; Mourier, B.; Susperrigui, A.-S.; Arnaud, F.; Bentaleb, I.; Chapron, E.; Lallier-Vergès, E.; Winiarski, T. 2011. Spectrocolorimetric interpretation of sedimentary dynamics: The new "Q7/4diagram". *Earth-Science Reviews*, 109: 1-19.

Demattê, J.A.M.; Garcia, G.J. 1999. Alteration of soil properties through a weathering sequence as evaluated by spectral reflectance. *Soil* Science *Society of America Journal,* 63: 327-342.

Djuwansah, M. 1990. *Mangroves de la zone equatorial. Estude sedimentologique, mineralogique et geochimique*. PhD Thesis. Strasbourg. Université Louis Pasteur. U.F.R dês Sciences de La Vie et de La Terre-Institut de Geologie. 124 p.

Fernandes, R.B.A.; Barrón, V., Torrent, J.; Fontes, M.P.F.R. 2004. Quantificação de óxidos de ferro de Latossolos brasileiros por espectroscopia de refletância difusa. *Revista Brasileira de Ciências do Solo*, 28: 245-257.

Fisch, G., Marengo, J.A., Nobre, C.A. 1998. Uma revisão geral sobre o clima da Amazônia. *Acta Amazonica*, 28: 101-126.

Gallo, M.N.; Vinzon, S. 2005. Generation of over tides and compound tides in Amazon estuary. *Ocean Dynamics*, 55: 441-448.

Galvão, L.S.; Vitorello, I. 1998. Role of organic matter in obliterating the effects of iron on spectral reflectance and colour of Brazilian tropical soils. *International Journal of Remote Sensing*, 19: 1969-1979.

Guimarães, J.T.F.; Cohen, M.C.L.; França, M.C.; Lara, R.J.; Behling, H. 2010. Model of wetland development of the Amapá coast during the late Holocene. *Anais da Academia Brasileira de Ciências*, 82: 451-465.

Guimarães, J.T.F.; Cohen, M.C.L.; Pessenda, L.C.R.; França, M.C., Smith, C.B.; Nogueira, A.C.R. 2012. Mid and late Holocene sedimentary process and palaeovegetation changes near the mouth of the Amazon River. *The Holocene*, 22: 359-370.

Henderson, R.E.; Patrick, J.R.W.H. 1982. Soil aeration and plant productivity. In: Rechcigl, Jr. M. (Ed.), *Handbook of Agricultural Productivity*, vol. 1. CRC Press, Boca Ratom, p. 51-69.

Hering, E. 1964. *Outlines of a theory of the light sense*. Harvard University Press, 344 p.

Lalonde, K.; Mucci, A.; Quellet, A.; Gélinas, Y. 2012. Preservation of organic matter in sediments promoted by iron. .*Nature*, 483: 198-200.

Kretz, R. 1983. Symbols for rock-forming minerals. *American Mineralogist*, 68: 277-279.

Leach, C.J.; Wagner, T.; Jones, M.; Juggins, S.; Stevenson, A. 2008. Rapid determination of total organic carbon concentration in marine sediments using Fourier transform near-infrared spectroscopy (FT-NIRS). *Organic Geochemistry*, 39: 910-914.

Malley, D.F.; Lockhart, L.; Wilkinson, P.; Hauser, B. 2000. Determination of carbon, carbonate, nitrogen and phosphorous in freshwater sediments by near-infrared reflectance spectroscopy: rapid analysis and a check on conventional analytical methods. *Journal of Paleoliminology*, 24: 415-425.

Meade, R.H.; Dunee, T.; Richey, J.E.; Santos, U.M.; Salati, E. 1985. Storage and remobilization of suspended sediment in the lower Amazon River of Brazil. *Science*, 228: 488-490.

Menezes, M.P.M.; Berger, U.; Mehlig, U. 2008. Mangrove vegetation in Amazonia: a review of studies from the coast of Pará and Maranhão States, north Brazil. *Acta Amazonica*, 38: 403-420.

Miall, A.D. 1978. Facies types and vertical profile models in braided river deposits: a summary. In: Miall, A.D. (Ed.) *Fluvial Sedimentology*. Calgary: Canadian Society of Petroleum Geologists, 597-604.

Moraes, B.C.; Costa, J.M.N.; Costa, A.C.L. 2005. Variação espacial e temporal da precipitação no estado do Pará. *Acta Amazonica*, 35: 207-214.

Munsell Color. 2009. *Geological Rock-Color Charts with genuine Munsell color ships*. Munsell Color X-rite. Grand Rapids, MI, USA.

Nascimento, M.S.; Góes, A.M. 2007. Petrografia de arenitos e minerais pesados de depósitos cretáceos (Grupo Itapecuru), Bacia de São Luís-Grajaú, norte do Brasil. *Revista Brasileira de Geociências*, 37: 50-63.

Ortiz, J.D.; Polyak, L.; Grebmeier, J.M.; Darby, D.; Eberl, D.D.; Naidu, S.; Doron, N. 2009. Provenance of Holocene sediment on the Chukchi-Alaskan margin based on combined diffuse spectral reflectance and quantitative X-Ray Diffraction analysis. *Global and Planetary Change*, 68: 73-84.

Rossel, R.A.V.; Minasny, B.; Roudier, P.; Mcbratney, A.B. 2006. Colour space models for soil science. *Geoderma*, 133: 320-337.

Rossetti, D.F.; Truckenbrodt, W. 1997. Revisão estratigráfica para os depósitos do Albiano-Terciário Inferior (?) na Bacia de São Luís, Maranhão. *Boletim do Museu Paraense Emílio Goeldi*, 9: 29-41.

Rossetti, D.F. 2001. Late Cenozoic sedimentary evolution in northeastern Pará, Brazil, within the context of sea level changes. *Journal of South America Earth Science*, 14: 77-89.

Rossetti, D.F.; Almeida, S.; Amaral, D.D.; Lima, C.M.; Pessenda, L.C.R. 2010. Coexistence of forest and savanna in an Amazonian area from a geological perspective. *Journal of Vegetation Science*, 21: 120-132.

Stigler, S.M. 1989. Francis Galton's Account of the Invention of Correlation. *Statistical Science* 4: 73-79.

Tiner, R.W. 1999. *Wetland Indicators: A Guide to Wetland Identification, Delineation, Classification, and Mapping*. CRC Press LLC. 399 p.

Tucker, M.E. 2003. *Sedimentary rocks in the field*. Wiley-Interscience 3rd ed, NewYork, 244 p.

Turekian, K.K.; Wedepohl, K.H. 1961. Distribution of the elements in some major units of the Earth´s crust. *Geological Society of America Bulletin*, 72: 175–192.

Vilhena, M.P.S.P.; Costa, M.L.; Berrêdo, J.F. 2010. Continental and marine contributions to formation of mangrove sediments in an eastern Amazonian mudplain: The case of the Marapanim estuary. *Journal of South America Earth Science*, 29: 427-438.

Walker, R.G. 1992. Facies, facies models and modern stratigrahic concepts. In: Walker, R.G. and James, N.P. (Eds.) *Facies Models - Response to Sea Level Change*. Ontario: Geological Association of Canada, 1-14.

Wedepohl, K.H. 1995. The composition of the continental crust. *Geochimica et Cosmochimica Acta,* 59: 1217-1232.

Recebido em: 23/12/2011
Aceito em: 14/08/2012